Viscous Wave Breaking and Ligament Formation in Microfluidic Systems

Xiaoyi Hu and Thomas Cubaud*
Department of Mechanical Engineering, Stony Brook University, Stony Brook, New York 11794, USA

(Received 15 March 2018; revised manuscript received 13 June 2018; published 27 July 2018)

Rapid layering of viscous materials in microsystems encompasses a range of hydrodynamic instabilities that facilitate mixing and emulsification processes of fluids having large differences in viscosity. We experimentally study the stability of high-viscosity stratifications made of miscible and immiscible fluid pairs in square microchannels and characterize the propagation dynamics of interfacial waves, including breaking and viscous ligament entrainment from wave crests at moderate Reynolds numbers. For large viscosity contrasts, parallel fluid streams adopt widely different velocities and provide a simple model system to probe the role of inflectional instabilities of stratified microflows in relation with classic inviscid-stability theory. We reveal novel viscous wave regimes and unravel dispersion relationships in the presence and absence of interfacial tension. Detailed examination of wave celerity shows the existence of optimal operation conditions for passively disturbing miscible fluid flows and continuously dispersing low-and high-viscosity fluids at the small scale.

DOI: 10.1103/PhysRevLett.121.044502

Irregular fluid motion has long been a source of inspiration and inquiry from the dancing of flames in a fire to the breaking of waves on shores. In confined systems, the appearance of sinuous flow paths indicates the transition to turbulence and the possibility to enhance mixing at large Reynolds numbers [1]. The amplification of disturbances from inflection points in velocity profile is a common hydrodynamic destabilization process [2]. As two fluids in relative motion typically involve inflection points, propagating perturbations at fluid interfaces—or waves—encompass a rich collection of fluid phenomena, including Rossby [3] and Kelvin-Helmholtz [4] waves in the atmosphere, and rogue waves [5] in open water. At the small scale, capillary waves [6,7] and Plateau-Rayleigh instabilities [8,9] have been widely investigated between immiscible fluids. In general, wave phenomena provide useful mechanisms to disperse fluids. In microchannels, natural instabilities of viscosity-stratified flows [10] are promising for the development of novel microfluidic mixing methods that do not necessitate active forcing to destabilize streams [11]. Linear and nonlinear stability analyses of viscous stratifications often involve solving the Orr-Sommerfeld equation in various wave-number ranges [12–15] and simple predictions of wave characteristics are not readily available. Although a few wavy flow patterns associated with the shear-induced instability of viscosity-differing fluids in bounded systems have been experimentally identified, such as pearl-mushroom [16] and bamboo waves [17] in core-annular flows, and small-amplitude waves [18] in Couette flows, systematic measurements of neutrally stable wave characteristics caused by inflectional instabilities and predicted by the classic inviscid-stability theory [19,20] remain challenging.

Here, we experimentally characterize the behavior of viscous waves in the basic configuration of two-layer flow in a square microchannel. We substantiate the dispersion relationship of inertial viscous waves, which significantly

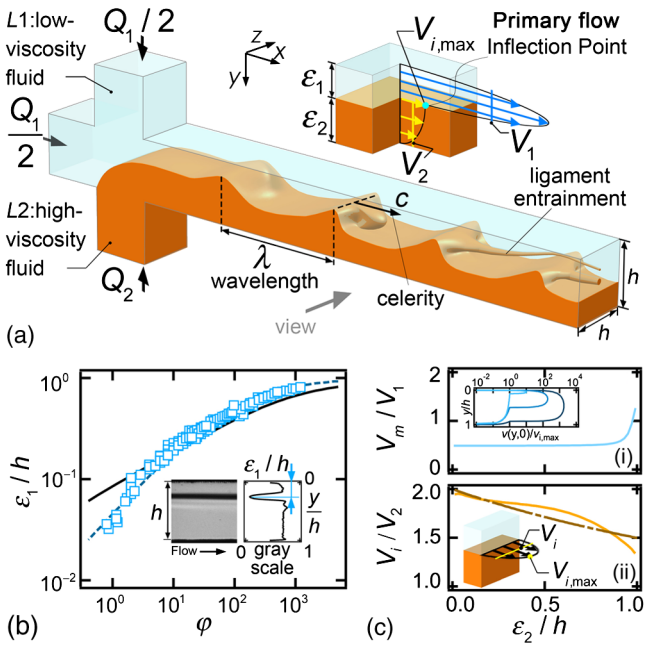

FIG. 1. (a) Schematics of traveling waves and viscous ligaments in a square microchannel. Inset: Velocity profile of primary flow. (b) Evolution of ε_1/h with φ for stable miscible stratifications. Inset: measurement of ε_1. Solid line: Eq. (1), dashed line: $\varepsilon_1/h = (1 + 2/3\varphi^{-2/3}\chi^{-1/2})^{-1}$. (c) Characteristic velocities of viscous stratifications: (i) average stream velocity V_m/V_1, (ii) interfacial velocity V_i/V_2, dot-dashed line: Eq. (2).

 © 2018 American Physical Society

differs from that of capillary waves. To generate stratifications, we employ silicon and glass microchannels with a hydrodynamic focusing section where a fluid $L1$ of viscosity η_1 is injected through the central and top channels at a total volume flow rate Q_1 and a more viscous fluid $L2$ of viscosity η_2 is introduced through the bottom channel at Q_2 [Fig. 1(a)]. The microchannel is placed on top of an inverted microscope equipped with a high-speed camera for image analysis. Both miscible and immiscible fluid pairs are used to characterize the influence of fluid properties on wave dynamics. The more viscous fluid $L2$ remains fixed in both cases and is made of silicone oil with a viscosity $\eta_2 = 485$ cP and density $\rho_2 = 0.97$ g mL^{-1}. For the miscible fluid pair, $L1$ consists of a low-molecular weight silicone oil of viscosity $\eta_1 = 0.49$ cP and density $\rho_1 = 0.76$ g mL^{-1} and the diffusion coefficient between the two oils is $D = 5.6 \times 10^{-10}$ m^2 s^{-1}. In the case of the immiscible fluid pair, $L1$ is made of ethanol with $\eta_1 = 1.08$ cP and $\rho_1 = 0.78$ g mL^{-1} and the interfacial tension is $\gamma = 1.09$ mN m^{-1}.

To characterize unstable regimes, we first analyze stable flow configurations [Fig. 1(a), inset] to determine reference interface location and characteristic velocities based on control parameters. In particular, we examine the relationship between the low-viscosity stream width ε_1 and quantities such as viscosity ratio $\chi = \eta_1/\eta_2$ and flow rate ratio $\varphi = Q_1/Q_2$. As the interface is slightly curved due to fluid self-lubrication effects [17], the width ε_1 is estimated from gray-scale profiles and is found in good agreement with a correlation previously developed for three-layer flows [10]. While the interface location ε_1 can be experimentally determined, a theoretical approach is needed to estimate average and interfacial velocities. Assuming a flat interface, we calculate velocity field and flow rate in each stream as a function of χ and ε_1 through Fourier analysis [21,22]. In the Supplemental Material [23], we rationalize computations and graphically establish the expression,

$$\varepsilon_1/h = [1 + 0.5(\varphi\chi)^{-1/2}]^{-1}, \tag{1}$$

which provides good experimental agreement with $\chi \sim 10^{-3}$ for $\varepsilon_1 > 0.1h$, when interfacial curvature effects can be neglected [Fig. 1(b)]. The average velocity in each stream is calculated as $V_1 = Q_1/(\varepsilon_1 h)$ and $V_2 = Q_2/(\varepsilon_2 h)$, with $\varepsilon_2 = h - \varepsilon_1$. Therefore, according to Eq. (1), $V_1/V_2 = 0.5(\varphi/\chi)^{1/2} \gg 1$ for very low χ and the low-viscosity stream is much faster than the high-viscosity stream. The average stream velocity $V_m = (V_1 + V_2)/2$ then scales with V_1 and is relatively independent of ε_2 [Fig. 1(c)(i)]. By contrast, the interfacial velocity V_i corresponds to the inflection point velocity and depends on flow features of both low- and high-viscosity fluid streams. We develop an analytical relationship for V_i by approximating computed square duct confinement with a parallel plates model [23], which yields

$$V_i = 6V_2/(3 + \varepsilon_2/h), \tag{2}$$

when $\chi \ll 1$ [Fig. 1(c)(ii)]. In the following, we use V_1 and V_i as characteristic velocities during the study of unstable layers.

Miscible and immiscible viscosity stratifications develop into a variety of flow regimes [Fig. 2]. Flow maps based on injection flow rates Q_1 and Q_2 provide a basis for directly comparing the influence of control parameters on flow patterns in the presence and in the absence of interfacial tension. For the miscible fluid case, four generic flow morphologies include (i) a diffusive regime with a vanishing interface for low flow rates, (ii) a stable regime with a straight interface for moderate flow rates, (iii) an inertial regime with a wavy interface, and (iv) viscous ligament entrainment from wave crests at large flow rates [Fig. 2(a)]. Transitions between regimes are delineated with specific dimensionless groups, such as the interfacial Péclet number, $\mathrm{Pe} = V_i h/D \approx 400$ between diffusive and stable regimes and the Reynolds number associated with the fast stream $\mathrm{Re}_1 = \rho V_1 h/\eta_1 \approx 96$ between the stable and inertial regimes. The Péclet number is a useful parameter to compare convective and diffusive transport of species in coflowing streams having similar viscosities [24,25]. Here, as streams have very large difference in velocity, we use V_i to characterize convection associated with the interfacial region. In the inertial regime, further increase in flow rates eventually leads to viscous wave breaking with ligament entrainment from

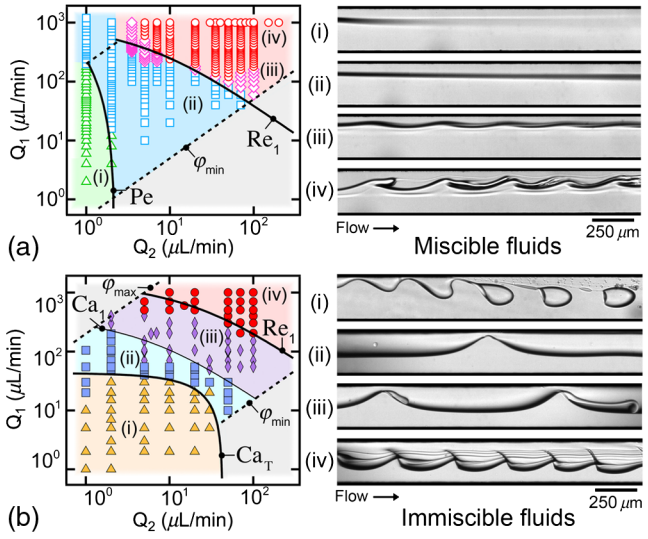

FIG. 2. Flow maps for miscible and immiscible fluids with corresponding experimental micrographs, flow rates in μl min^{-1} (a) Miscible fluid pair with (i) diffusive $(Q_1, Q_2) = (20, 1)$ (triangle), (ii) stable (100, 5) (square), (iii) transitional (180, 20) (diamond), and (iv) inertial viscous wave (1000, 70) (circle) regimes with $\varphi_{\max} = 500$ and $\varphi_{\min} = 0.5$ (b) Immiscible fluid pair including (i) droplet (5, 30) (filled triangle), capillary (ii) smooth (55, 20) (filled square) and (iii) broken viscous wave (205, 20) (filled diamond), and (iv) inertial viscous wave (505, 20) (filled circle) regimes with $\varphi_{\max} = 200$ and $\varphi_{\min} = 0.15$. See main text for transition curves.

the high-viscosity fluid to the low-viscosity stream. In both cases, the spatial period of undulations remains nearly constant $\lambda/h \approx 1.8$ and corresponds to a wave number $k = 2\pi/\lambda \approx 14$ mm^{-1} [Fig. 3(a)]. The critical average velocity V_1 associated with the fast stream follows a simple scaling, which is deduced using Eq. (1) such as $V_1 \approx 0.5Q_1(\varphi\chi)^{-1/2}/h^2 = 0.5(Q_1Q_2)^{1/2}\chi^{-1/2}/h^2$ since $(\varphi\chi)^{-1/2} \gg 1$ for $\varphi < 20$. Thus, the critical velocity $V_1 \sim (Q_1Q_2)^{1/2}$ corresponds to the geometrical mean of injection flow rates. Graphical analysis of flow maps in the Supplemental Material [23] provides further insights for the choice of characteristic velocities associated with specific transitions.

Regimes associated with the immiscible fluid pair include four flow archetypes, including (i) droplet formation at low flow rates, (ii) smooth long wave pattern for modest flow rates, (iii) ligament emitting waves for moderate flow rates, and (iv) inertial waves for large flow rates [Fig. 2(b)]. The droplet regime is specific to immiscible fluid pairs convected at relatively low flow rates in microsystems [9] and here corresponds to the situation where the low-viscosity stream becomes encapsulated by $L2$ to form a segmented flow of small droplets [Fig. 2(b)(i)]. As droplets are lifted from the walls to the center axis

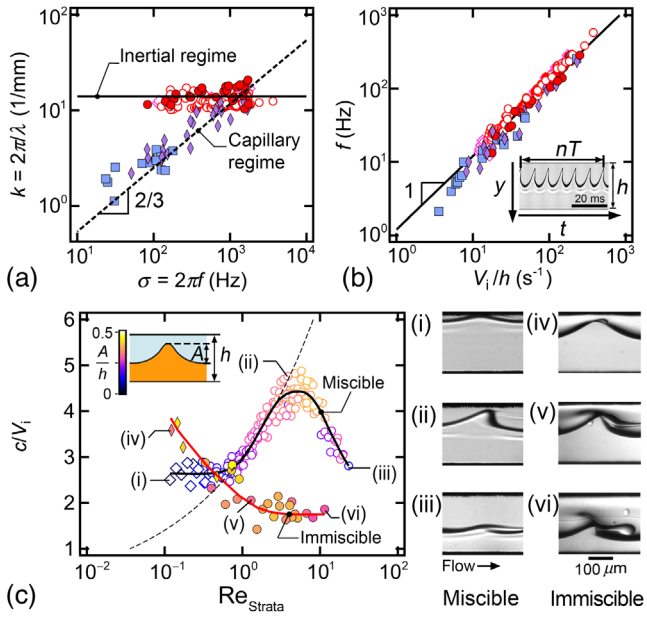

FIG. 3. Wave dynamics. (a) Dispersion relationship between wavenumber $k = 2\pi/\lambda$ and angular frequency $\sigma = 2\pi f$ for capillary and inertial regimes, dashed line: $k = [(\rho_1 + \rho_2)/\gamma]^{-1/3}\sigma^{2/3}$; solid line: $k = 14$ mm^{-1}. (b) Measured wave emission frequency f as a function of interfacial shear rate V_i/h for all waves. Solid line: $f = 1.25V_i/h$. Inset: example of spatiotemporal diagram used to measure f. (c) Normalized wave celerity as a function of $\mathrm{Re}_{\mathrm{strata}}$ for miscible and immiscible fluid pairs with corresponding micrographs. The color scale represents the wave height A/h. Dashed line: $c/V_i = 3\mathrm{Re}_{\mathrm{strata}}^{1/3}$.

of the channel due to the high-viscosity continuous phase, drops adopt a velocity near the average velocity $J_T = (Q_1 + Q_2)/h^2$. Above a critical J_T, viscous waves of long wavelengths ($\lambda \gg h$) are found to travel along the immiscible interface as predicted by linear stability analysis for any small Reynolds number [12]. To characterize this transition, J_T is normalized with the capillary velocity γ/η_2 of the encapsulating phase to form a critical capillary number $\mathrm{Ca}_T = \eta_2 J_T/\gamma \approx 5$. For separated flows, the onset of breaking waves with ligament emission occurs near a capillary number based on the fast stream, $\mathrm{Ca}_1 = \eta_1 V_1/\gamma \approx 0.1$ [Fig. 2(b)]. The appearance of entrainment at wave crests suggests the prevalence of deforming shear stress exerted by the low-viscosity stream over restoring interfacial tension stress. The wavelength of immiscible stratified flows is found to decrease with flow rates and the value of $\lambda/h \approx 1.8$ is reached above a critical $\mathrm{Re}_1 \approx 81$ indicating transition to inertial regimes similar to the miscible fluid case. Each wave crest then emits a thin ligament that is significantly stretched in the fast low-viscosity stream and transported outside of the wave structure. Further downstream, the progressive depletion of the viscous stream width ε_2 indicates significant transport of high-viscosity fluid through ligaments.

Important physical aspects of traveling waves include frequency f, wavelength λ, celerity c, and amplitude A. The space-time coherence of undulations is typically captured using a dispersion relationship, which associates angular frequency $\sigma = 2\pi f$ and wave number $k = 2\pi/\lambda$. Here, data for long wave regimes are found in good agreement with capillary wave theory [26] according to $k = [(\rho_1 + \rho_2)/\gamma]^{-1/3}\sigma^{2/3}$ for immiscible fluids [Fig. 3(a)]. For larger wave numbers $k = 14$ mm^{-1}, the inertial regime is characterized with a wavelength λ that remains independent of frequency f for both miscible and immiscible fluid pairs [Fig. 3(a)]. Incidentally, in confined microsystems the inertial regime displays smaller λ compared to capillary waves that are usually considered the lower limit of interfacial waves in open waters [27].

The wavelength λ provides a useful indicator of flow regimes and is related to frequency and celerity according to the basic wave equation $c = f\lambda$. Remarkably, we find direct proportionality between frequency f and interfacial velocity V_i for over two decades and for all stratified wave regimes with both miscible and immiscible fluid pairs according to $f = 1.25V_i/h$ [Fig. 3(b)]. The quantity V_i/h is useful as it can be calculated from control parameters and is interpreted as the characteristic interfacial shear rate. As V_i corresponds to the velocity of the inflection point, this simple result is in excellent agreement with the inviscid-stability theorem [19,28] and our experimental findings suggest a possible extension of the domain of validity to confined shear flow instabilities of viscous materials.

By contrast to the wave frequency f, the wave celerity c displays a nonmonotonic behavior with V_i for miscible

flows and the ratio c/V_i decreases in proportion to λ for immiscible flows since according to $c = f\lambda$ with $f \sim V_i$, one would expect $c/V_i \sim O(10^1)$ for long waves and $c/V_i \sim O(10^0)$ for inertial waves. To better understand variations of celerity c in inertial regimes and the influence of wave amplitude A, we examine the relationship between c/V_i and a stratification Reynolds number $\mathrm{Re}_{\mathrm{strata}} = \rho_1 V_1^2 \varepsilon_1/(\eta_2 V_2)$ based on the ratio of the inertial force associated with the fast stream $(\rho_1 V_1^2)(\varepsilon_1 h)$ and the shear force in the slow stream $(\eta_2 V_2/\varepsilon_2)(\varepsilon_2 h)$ [Fig. 3(c)]. While Re_1 is useful for predicting transition to inertial regimes, the stratification Reynolds number $\mathrm{Re}_{\mathrm{strata}}$ is helpful for comparing wave dynamics within inertial regimes and is similar to a theoretical argument on the growth rate of interfacial waves in Couette flow configuration [29]. Here, as the celerity c is independently measured from high-speed imaging and normalized with a velocity V_i, which is numerically calculated from control parameters Q_1 and Q_2, data reveal the fine influence of the wave amplitude A on flow behavior in the inertial regime. The wave height A is measured between crests and troughs and coded using a color scale to show correlations with c in Fig. 3(c). For the miscible fluid pair, small wave amplitudes, $A < 0.2h$, are observed for $\mathrm{Re}_{\mathrm{strata}} < 1$ and $c/V_i \approx 2.7$. Both maximal amplitude $A \approx 0.4h$ and celerity $c \approx 4.5V_i$ are reached for $\mathrm{Re}_{\mathrm{strata}} = 5$, following a scaling $c/V_i \approx 3\mathrm{Re}_{\mathrm{strata}}^{1/3}$ since a greater inertial force is exerted on wave crests for larger A and waves adopt higher c/V_i. A further increase of $\mathrm{Re}_{\mathrm{strata}}$ leads to a decrease of both A/h and c/V_i due to the apparent flattening effect of the strong inertial force associated with the low-viscosity stream. The presence of a maximum c/V_i suggests an optimum $\mathrm{Re}_{\mathrm{strata}}$ for mixing applications where viscous stratified flows made of miscible fluids can be most effectively disturbed over short distances. By contrast, the relative celerity of interfacial waves between immiscible fluids experiences a monotonic decline with $\mathrm{Re}_{\mathrm{strata}}$ and reaches a plateau $c \approx 1.8V_i$ in the inertial regime with no significant correlations between A and c. Beside these fine variations, the scaling $c \sim V_i$ is in good the agreement with classic inviscid-stability theorem [19].

We now turn our attention to the dynamics of viscous ligaments entrained from interfacial ridges in various flow regimes. Slender structures protrude from viscous waves as a result of a large discrepancy between the wave celerity $c \sim V_i$ and the low-viscosity fluid stream velocity $V_1 \gg V_i$. During propagation, viscous wave crests experience a straining force due to the fast side stream, which triggers breaking and ligament withdrawal. Entrainment of threads and tendrils involves complex mechanisms that have been studied in several different contexts [30–35]. In this work, we examine three typical entrainment dynamics of microfluidic waves including (i) capillary ligament yarning and inertial entrainment of (ii) miscible and (iii) immiscible fluid threads as presented in Fig. 4. In the inertial regimes, the front velocity of ligaments normalized by the wave

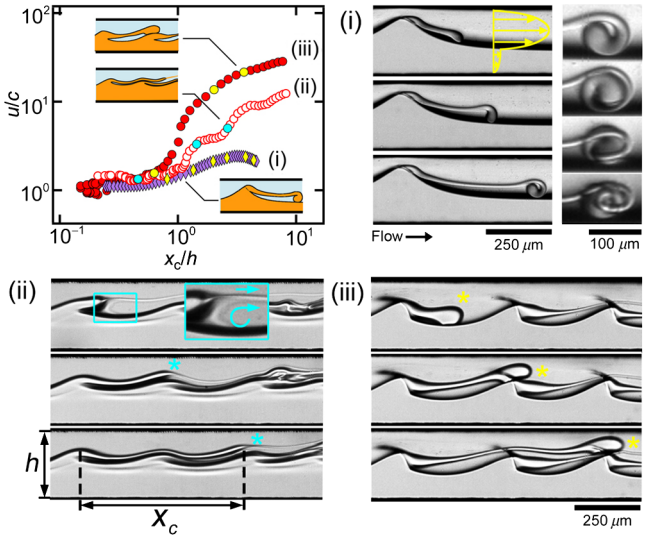

FIG. 4. Dynamics of ligament entrainment with evolution of front velocities in the reference frame of wave crests, flow rates in μl min^{-1}: (i) immiscible ligament yarning with $u/c \sim O(10^0)$ for $(Q_1, Q_2) = (20, 305)$ and inertial regimes with $u/c \sim O(10^1)$ for (ii) miscible fluid (20, 800) and (iii) immiscible fluid pairs (15, 600). Selected images correspond to solid data points on the velocity graph.

celerity u/c widely grows in the reference frame of the wave crest for both miscible and immiscible stratifications. In particular, ligaments are found to gain significant speed when they reach the next downstream crest as they are sworn into the bulk of the fast stream outside of the wave structure. By contrast, for midrange waves in the viscous capillary regime, the relative velocity of ligaments remains on the order of unity in the experimental field of view and ligaments display intriguing trundling behaviors that consist of a rolling mode due to the clockwise torque generated by local velocity profile in a wave trough. The small relative speed of ligament allows accumulation of viscous fluid at the tip, which rotates and form a structure suggesting a ball of yarn. Such phenomenon is unique to capillary viscous waves since tip rotation requires a long and flat trough, i.e., a large λ. For inertial viscous waves, when $u/c \sim O(10^1)$, multiple ligament entrainments are observed for both immiscible and miscible fluid pairs. As immiscible ligaments form well-defined rounded tips, they experience a larger drag compared to their slender miscible counterparts and, as a result, display larger velocities for similar flow rates. Complex flow structures including recirculating vortex are also observed with miscible fluids [Fig. 4].

In this letter, we report a set of complex yet periodic flow regimes arising from simple miscible and immiscible viscous stratifications in confined microsystems, including a long wave capillary regime and a short wave inertial regime. We find good agreement with theory for the dispersion relationship of capillary waves and we delineate the dispersion relationship of waves in the inertial regime

for both miscible and immiscible fluid pairs. In the inertial regime, the wavenumber remains constant regardless of frequency or interfacial tension, which allows us to clearly distinguish flow transitions. In addition, evidence of direct proportionality between experimental wave frequency and computed interfacial shear rate of primary flow confirms the role of inflectional regions during pressurized shear-flow instabilities for all stratified regimes. The interfacial velocity provides an intrinsic reference to examine the evolution of wave celerity as a function of the stratification Reynolds number. For the case of miscible stratifications, we show that the maximal relative celerity is reached for large wave amplitude suggesting the existence of optimal micromixing conditions through ligament entrainment. Overall, we shed light on numerous novel destabilizing processes and characterize flow transitions using dimensionless groups based upon confined high-viscosity fluid strata. Viscous ligaments emitted from wave crests can be employed to continuously blend small amounts of high-viscosity fluids with miscible solvents or disperse fine droplets into a low-viscosity continuous phase. Our study provides important practical elements to better manipulate a range of environmental, biological, and engineered multifluid flows with vast viscosity contrasts at the small scale. While capillary waves are usually seen as the smallest interfacial waves, our work shows the transition to smaller inertial waves in confined microsystems. Further fundamental work on the relationship between maximal wave number and confinement would improve our current understanding of intriguing viscous wave dynamics in confined microsystems.

This material is based upon work supported by the National Science Foundation under Grant No. CBET-1150389.

*To whom correspondence should be addressed.
thomas.cubaud@stonybrook.edu

[1] D. J. Tritton, *Physical Fluid Dynamics* (Oxford University Press, New York, 1988).
[2] R. Govindarajan, V. S. L'vov, and I. Procaccia, Phys. Rev. Lett. **87**, 174501 (2001).
[3] Y. Wang, A. Gozolchiani, Y. Ashkenazy, Y. Berezin, O. Guez, and S. Havlin, Phys. Rev. Lett. **111**, 138501 (2013).
[4] P. G. Drazin and W. H. Reid, *Hydrodynamic Stability* (Cambridge University Press, Cambridge, England, 2004).
[5] A. Toffoli, D. Proment, H. Salman, J. Monbaliu, F. Frascoli, M. Dafilis, E. Stramignoni, R. Forza, M. Manfrin, and M. Onorato, Phys. Rev. Lett. **118**, 144503 (2017).
[6] M. Shats, H. Punzmann, and H. Xia, Phys. Rev. Lett. **104**, 104503 (2010).
[7] É. Falcon, C. Laroche, and S. Fauve, Phys. Rev. Lett. **98**, 094503 (2007).
[8] P. Guillot, A. Colin, A. S. Utada, and A. Ajdari, Phys. Rev. Lett. **99**, 104502 (2007).
[9] S. L. Anna, Annu. Rev. Fluid Mech. **48**, 285 (2016).
[10] X. Hu and T. Cubaud, Phys. Rev. Fluids **1**, 044101 (2016).
[11] S. Y. Mak, Y. Chao, S. Rahman, and H. C. Shum, Langmuir **34**, 926 (2018).
[12] C.-S. Yih, J. Fluid Mech. **27**, 337 (1967).
[13] C. E. Hickox, Phys. Fluids **14**, 251 (1971).
[14] A. Hooper and W. Boyd, J. Fluid Mech. **128**, 507 (1983).
[15] R. Govindarajan and K. C. Sahu, Annu. Rev. Fluid Mech. **46**, 331 (2014).
[16] M. d'Olce, J. Martin, N. Rakotomalala, D. Salin, and L. Talon, Phys. Fluids **20**, 024104 (2008).
[17] D. Joseph and Y. Renardy, *Fundamentals of Two-Fluid Dynamics, Part II: Lubricated Transport, Drops and Miscible Liquids* (Springer, New York, 1993).
[18] M. Sangalli, C. T. Gallagher, D. T. Leighton, H. C. Chang, and M. J. McCready, Phys. Rev. Lett. **75**, 77 (1995).
[19] F. M. White and I. Corfield, *Viscous Fluid Flow* (McGraw-Hill, New York, 2006), Vol. 3.
[20] S. A. Maslowe, Annu. Rev. Fluid Mech. **18**, 405 (1986).
[21] W. E. Langlois and M. O. Deville, *Slow Viscous Flow* (Macmillan, New York, 1964).
[22] Z. Wu and N.-T. Nguyen, Biomed. Microdevices **7**, 13 (2005).
[23] See Supplemental Material at http://link.aps.org/supplemental/10.1103/PhysRevLett.121.044502 for primary flow model.
[24] R. F. Ismagilov, A. D. Stroock, P. J. A. Kenis, G. Whitesides, and H. A. Stone, Appl. Phys. Lett. **76**, 2376 (2000).
[25] J. B. Salmon and A. Ajdari, J. Appl. Phys. **101**, 074902 (2007).
[26] H. Lamb, *Hydrodynamics*, 6th ed. (Cambridge University Press, Cambridge, England, 1932).
[27] P. H. LeBlond and L. A. Mysak, *Waves in the Ocean*, Elsevier Oceanography Series 20 (Elsevier Scientific Pub. Co., Amsterdam, New York, 1978).
[28] C. Godrèche, P. Manneville, and B. Castaing, *Hydrodynamics and Nonlinear Instabilities* (Cambridge University Press, Cambridge England, 2005).
[29] E. J. Hinch, J. Fluid Mech. **144**, 463 (1984).
[30] P. Marmottant and E. Villermaux, J. Fluid Mech. **498**, 73 (2004).
[31] M. Ishii and M. Grolmes, AIChE J. **21**, 308 (1975).
[32] G. B. Deane and M. D. Stokes, Nature (London) **418**, 839 (2002).
[33] L. E. Schmidt and W. W. Zhang, Phys. Rev. Lett. **100**, 044502 (2008).
[34] L. O. Naraigh, P. Valluri, D. M. Scott, I. Bethune, and P. D. M. Spelt, J. Fluid Mech. **750**, 464 (2014).
[35] W. L. Olbricht, Annu. Rev. Fluid Mech. **28**, 187 (1996).